Motility-Induced Clustering of Active Particles under Soft Confinement

Timo Knippenberg,[1] Ashreya Jayaram,[2] Thomas Speck,[2,*] and Clemens Bechinger[1,†]

[1]*Fachbereich Physik, Universität Konstanz, 78464 Konstanz, Germany*
[2]*Institute for Theoretical Physics IV, University of Stuttgart, 70569 Stuttgart, Germany*

We investigate the structural and dynamic properties of active Brownian particles (APs) confined within a soft annulus-shaped channel. Depending on the strength of the confinement and the Péclet number, we observe a novel reentrant behavior that is not present in unconfined systems. Our findings are substantiated by numerical simulations and analytical considerations, revealing that this behavior arises from the strong coupling between the Péclet number and the effective confining dimensionality of the APs. Our work highlights the peculiarities of soft boundaries for APs and how clogging can be avoided under such conditions.

The spatial confinement of systems typically leads to changes of their physical and chemical properties (melting temperature, band structure, magnetic behavior, etc.) compared to their bulk behavior [1–3]. This also applies to groups of active, i.e., self-propelled, particles (APs), which constitute the novel class of active matter [4,5]. Systems composed of APs are distinguished by an intricate interplay between their local density and propulsion speed which gives rise to a motility-induced phase separation (MIPS) [6,7]. This phenomenon has been observed in a wide range of active systems including synthetic colloidal [8,9] and bacterial suspensions [10] and collectives of ants [11], and has been studied extensively in computer simulations [12–15].

Motivated by the fact that the natural environment of many living APs is dominated by geometrical confinements, e.g., porous media (soils) [16] or narrow blood vessels [17], recent studies have investigated their properties near surfaces [18,19], within channels [20], and confined to optical traps [21]. These studies demonstrate that spatial confinement has a pronounced influence on the behavior of APs promoting, e.g., the formation of lanes and bands [22]. Such confinement-induced behavior is also important in view of potential applications of synthetic APs such as embolization [17] or drug delivery [23]. As opposed to extensive work on APs in bulk and near *hard* walls and channels, however, only few studies have investigated the behavior of APs confined by *soft* boundaries. In particular when APs are confined to a soft one-dimensional channel, AP fluctuations perpendicular to the channel will increase with increasing propulsion velocity v. This leads to a v-dependent effective dimensionality to which the system is confined. Because MIPS has been demonstrated to be largely suppressed [24,25] for one-dimensional (1D) confinements (as opposed to higher dimensions [12,26–28]), this suggests a nontrivial phase behavior of APs in soft confinements as a function of their propulsion velocity.

In this Letter, we experimentally and numerically study the clustering of APs in a narrow annular channel created by two concentric soft repulsive barriers. By varying the softness of these barriers and the velocity v of the APs, we can systematically tune the effective dimensionality of the system from one (single-file) to two spatial dimensions (2D). Upon increasing the AP propulsion velocity or the softness of the confinement, we find a transition from a homogeneous to an inhomogeneous cluster phase and eventually back to a homogeneous AP distribution within the annulus. Such reentrant behavior is a unique feature of soft confinements and finds no resemblance in 2D systems where phase separation persists for all activities above the critical point.

In our experiments, we use N active Janus particles composed of silica spheres (diameter $\sigma = 7.8$ µm) coated with a 60 nm thick carbon layer on one hemisphere. Owing to gravitational and hydrodynamic forces, their motion is restricted to the lower bottom of the sample cell. When suspended in a critical binary mixture of water and propylene-glycol-n-propyl ether (40% m) and illuminated with a laser beam ($\lambda = 532$ nm), the carbon caps are selectively heated. This leads to an asymmetric demixing of the fluid around the particle [29,30]. As a result, the particles perform an active Brownian motion whose propulsion velocity v is controlled by the laser intensity. In our experiments we use a single laser beam which is permanently scanned over all APs and focused on their carbon cap. In the following, we use the Péclet number Pe $\equiv 3v/(D_R\sigma)$ to characterize v with the rotational diffusion coefficient $D_R \approx 0.001\,25$ s^{-1}; see the Supplemental Material [31].

*Contact author: thomas.speck@itp4.uni-stuttgart.de
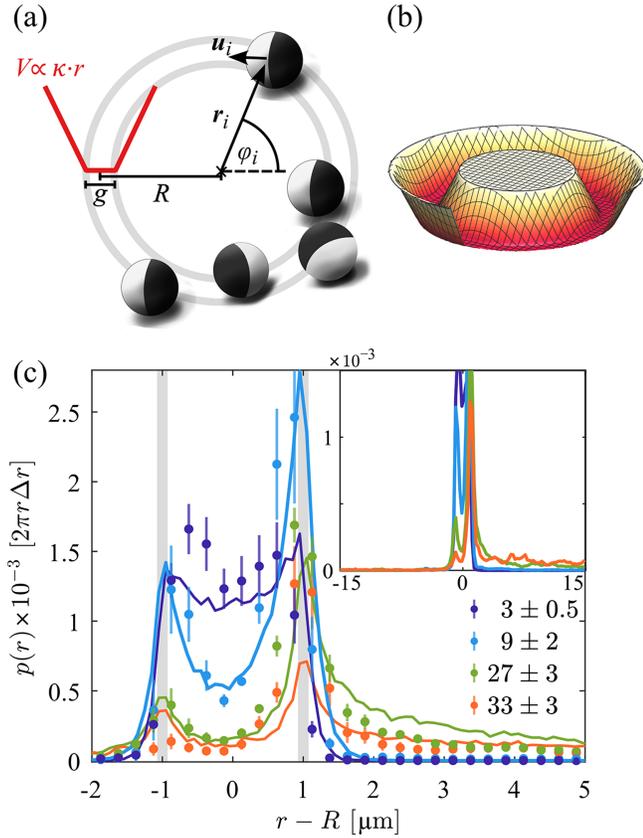†Contact author: clemens.bechinger@uni-konstanz.de

FIG. 1. (a) Schematic view of APs confined to an annular-shaped confinement, the latter providing an effective potential, acting with respect to the center of mass of the confined APs. The cross section is sketched in red, and the whole potential is shown in (b). (c) Radial position probability density $p(r)$ of a single AP inside the confinement for different Pe and constant confinement strength. $p(r)$ is normalized by bin width $\Delta r = 0.25$ μm and circumference. Circles refer to experimental data, while lines show the corresponding curves from simulations. In the simulations, $\kappa = 70(k_{\mathrm{B}}T/\sigma)$ (see below) and Pe = 3, 9, 27, 30. The gray vertical lines indicate the onset of the soft confining walls at $r = R \pm (g/2)$. The inset shows the same curves for the range $r - R = [-15, 15]$ μm.

To generate soft barriers for an AP, we take advantage of its negative phototactic behavior, i.e., the fact that the APs are effectively repelled away from a positive light intensity gradient [33]. Technically, such a repulsive barrier can be created by the application of an additional laser light gradient near the edge of an AP, once its center of mass crosses a virtually specified boundary [34,35]. This approach allows one to generate a constant repulsive force whose strength κ can be controlled by the magnitude of the applied light gradient. In our experiments, the boundaries are two concentric rings with radii $R \pm g/2$ where $R = 55$ μm and a gap of width $g = 2$ μm in between [see in Fig. 1(a)]. In total, this can be represented by an annulus shaped, linear, confining potential $V(r)$ with slopes κ and a force free gap [Fig. 1(b)] (see the Supplemental Material [31] and below

for further details). Notably, in contrast to a topographical confinement, this approach avoids the influence of hydrodynamic interactions with the boundaries.

To experimentally demonstrate the creation of adjustable soft confinements, we determined the radial density $p(r)$ of a single AP, which quantifies the radial localization of APs to the annular-shaped potential, as a function of Pe and the confinement strength κ. A detailed discussion of how κ is obtained experimentally is given below and in the Supplemental Material [31]. The experimentally measured data are shown in Fig. 1(c). At fixed κ and Pe = 3, $p(r)$ is distributed narrowly around $r = R$. For larger Pe the APs are able to increasingly move toward the repulsive barriers which leads to an increasing width of $p(r)$. In addition, two maxima at $r \approx R \pm 1$ μm appear. They result from the AP accumulation at the inner and outer soft boundary, similar to what is known for their behavior near hard walls [18,36,37]. Moreover, as Pe grows, $p(r)$ becomes highly asymmetric with a tail toward the outer confinement. This is due to the preference of APs to accumulate at concave rather than convex boundaries [38,39]. A comparable behavior is observed when Pe is fixed and κ is varied (see the Supplemental Material [31]).

In addition to experiments, we also performed numerical simulations where APs are modeled as active Brownian particles moving in 2D. The dynamics of the position $\mathbf{r}_i$ and orientation ϑ_i of the ith AP is governed by

$$\dot{\mathbf{r}}_i = v\mathbf{u}_i + \frac{D_{\mathrm{T}}}{k_{\mathrm{B}}T}(-\nabla V_{\mathrm{WCA}} + \mathbf{f}_i) + \sqrt{2D_{\mathrm{T}}}\boldsymbol{\zeta}_{\mathrm{T},i} \qquad (1)$$

$$\dot{\vartheta}_i = M\sum_{j \in \Omega_i} \sin\left[2(\vartheta_j - \vartheta_i)\right]\Pi(\vartheta_i, \vartheta_j) + \sqrt{2D_{\mathrm{R}}}\zeta_{\mathrm{R},i}, \qquad (2)$$

where unit orientation vector $\mathbf{u}_i \equiv (\cos\vartheta_i, \sin\vartheta_i)^T$ and D_{T} is the translational diffusion constant. The components of $\boldsymbol{\zeta}_{\mathrm{T},i}$ and $\zeta_{\mathrm{R},i}$ are obtained from a unit normal distribution (i.e., zero mean and unit variance). The APs interact via the repulsive short-range Weeks-Chandler-Anderson (WCA) potential V_{WCA} [40] modeling volume exclusion. Going beyond the standard model of active Brownian particles, we anticipate lubrication effects to play a major role in a strongly confined system. Previous works on squirmers [41,42] and Quincke rollers [43] indicate that these interactions prompt an effective alignment between APs. To account for this, we additionally impose an aligning torque of strength M. We find that a choice of $M = 10^4 D_{\mathrm{R}}$ results in good agreement between simulations and experiments as discussed below. The indicator function $\Pi(\vartheta_i, \vartheta_j)$ is unity if the relative orientation of the two APs is between $\pi/2$ and $3\pi/2$ and zero otherwise. The total torque on the ith AP is then the sum over all pairwise torques exerted due to neighboring particles within a circular region Ω of radius $2^{1/6}\sigma$ centered at $\mathbf{r}_i$. We model the confining force on the ith AP as
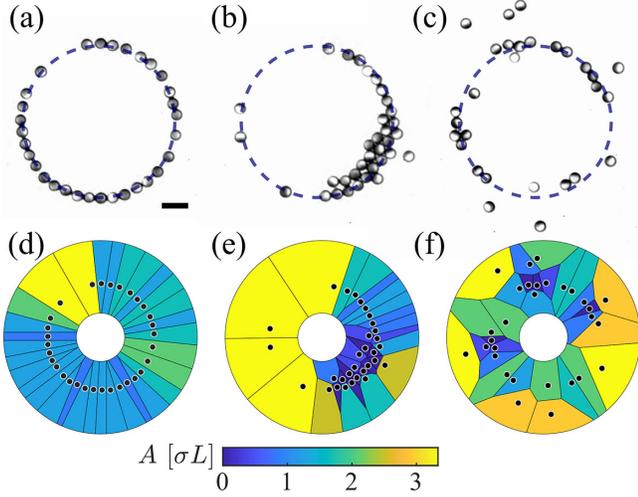
FIG. 2. Representative microscopy images for (a) Pe = 3, (b) 27, (c) 33. The scale bar represents 20 μm. The dashed lines indicate the channel. (e)–(f) Show the corresponding Voronoi tessellations. Colors denote the area A of the Voronoi cells.

$$\mathbf{f}_i = \begin{cases} \kappa \mathbf{e}_{r,i} & \text{if } |\mathbf{r}_i| < \left(R - \frac{g}{2}\right) \\ -\kappa \mathbf{e}_{r,i} & \text{if } |\mathbf{r}_i| > \left(R + \frac{g}{2}\right) \\ 0 & \text{otherwise,} \end{cases} \quad (3)$$

with $\mathbf{e}_{r,i} \equiv (\cos \varphi_i, \sin \varphi_i)^T$ the normal vector.

When several APs are placed in such a soft annular channel, the interplay of confinement and self-propulsion determines the phase behavior of the APs. Representative snapshots of the steady state for constant barrier strength κ and increasing Pe are shown in Figs. 2(a)–2(c) and are obtained for $N = 30$. To quantify the particle density, we introduce the filling fraction $\phi \equiv N\sigma/(2\pi R)$, which yields for our experimental conditions $\phi \simeq 0.68$. At Pe = 3, APs are effectively confined to 1D (single file conditions) with only little radial fluctuations. Particles organize into chains which permanently break up into fragments and reform (see the Supplemental Material, Videos 1 and 2). Such behavior is in good agreement with previous studies that confirm the absence of macroscopic phase separation of APs in 1D channels [24]. Upon increasing Pe to Pe = 27, APs are able to pass each other and form multilayered, dense dynamical clusters which coexist with a surrounding gas phase (see the Supplemental Material, Video 3). For the conditions shown here, these clusters are comprised of typically more than half of the APs, and they are stable over timescales of several D_R^{-1}). Such behavior is comparable to MIPS in 2D systems. Note, however, that phase separation in our experiments is observed for Pe values below the critical speed Pe $\gtrsim 40$ of 2D bulk systems [26]. At the largest Pe achieved in our study (Pe = 33), the radial fluctuations of APs further increase which reduces their effective density (see the Supplemental Material, Video 4). Similar to 2D systems where MIPS is absent at low densities, also in our
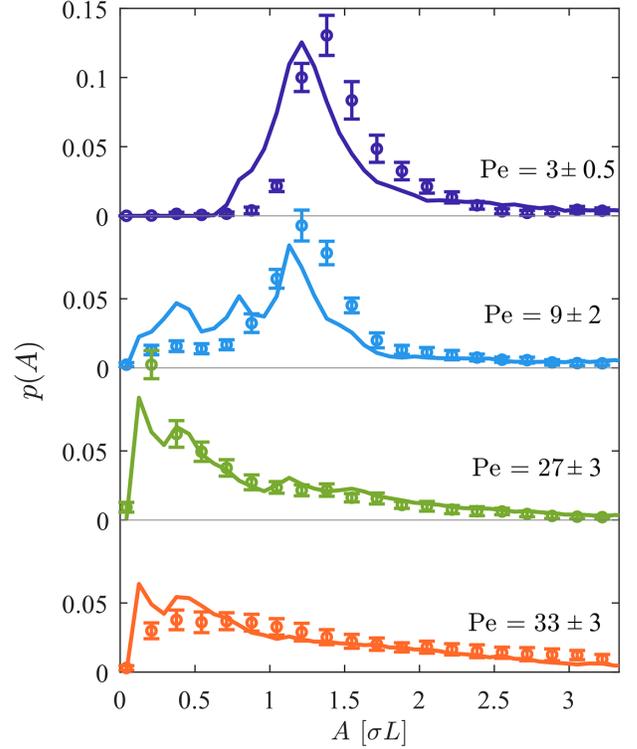

FIG. 3. Probability distribution $p(A)$ of Voronoi cell areas for different Pe and $\kappa = 110 k_B T/\sigma$, $N = 30$. Lines represent simulated data, while circles denote experimental data.

case the clusters disappear and the system becomes more homogeneous in the angular direction.

To quantify the Pe-dependent changes of the AP behavior, we perform a Voronoi tessellation. We restrict the evaluation to an annulus-shaped area whose inner (R_i) and outer (R_a) radii have been chosen to be sufficiently large to include all APs independent of Pe (here, $L = R_a - R_i = 9.6\sigma$). Figures 2(d)–2(f) show the corresponding Voronoi cells to Figs. 2(a)–2(c) where the Voronoi areas A are colored according to their values. The time-averaged (each measurement was averaged over $\approx 36 D_R^{-1}$) probability distribution $p(A)$ is shown in Fig. 3. For Pe = 3 and 9, $p(A)$ is rather narrow which indicates that APs are homogeneously spread in the angular direction within the annulus. With increasing Pe = 27, this peak gradually disappears at the expense of a maximum which develops at small A exhibiting a long tail toward larger values. Such behavior indicates the presence of an AP cluster. At the largest Pe = 33 the maximum shrinks, leading to a rather more uniform $p(A)$. This corresponds to a random distribution [44] of APs within the annulus [Fig. 2(f)].

Comparable results are also obtained from our numerical simulations. The presence of a lubrication-induced torque ($M \neq 0$) is crucial to enable the escape of APs in the lateral direction upon direct collisions. This promotes the formation of multilayer clusters in agreement with our experiments. To determine the value of the confinement strength
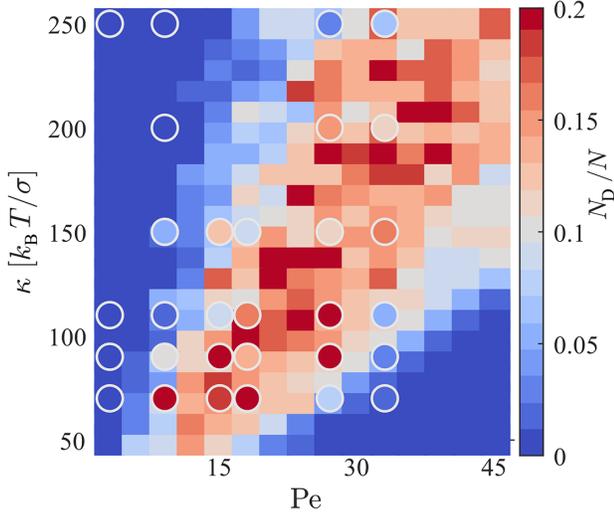
FIG. 4. Phase diagram showing the fraction of APs in a dense surrounding $\langle N_D/N \rangle$ for different κ and Pe. Here $N = 30$. The rectangles are simulation data, and the circles represent experiments.

in our experiment, we have varied κ in the numerical simulations until best agreement with the Voronoi area distributions of the experimental data has been achieved (see Fig. 3, and see the Supplemental Material [31] for details on the comparison procedure.) As a confirmation of this approach, we have calculated the radial particle distribution $p(r)$ for the conditions shown in Fig. 1(c). Using the κ value obtained with the above procedure yields good agreement with the experiments.

In Fig. 4, we show the phase diagram of APs in an annular confinement as a function of κ and Pe as obtained from experimentally measured data and numerical simulations. As an order parameter to characterize the presence of clusters, we have measured the fraction $\langle N_D/N \rangle$ of APs having a Voronoi area below a threshold value [16]. In our case this threshold was set to be a bit larger than the corresponding value for a 2D random close packing ($A_{RCP} \approx 1.02\sigma^2$ [45]) to accommodate its distribution width. This led us to $A < 0.2\sigma L \approx 2\sigma^2$. Clearly, cluster formation is limited to a diagonal region in the κ-Pe space which suggests a reentrant behavior along both axes. A similar behavior was also found for $N = 46$ ($\phi \simeq 1.04$), i.e., slightly overcrowded systems (see the Supplemental Material [31]).

We can rationalize the phase diagram in Fig. 4 from simple geometric considerations. To focus on the essential ingredients, we consider a flat channel confined by constant perpendicular forces with strength κ. Mathematically, this problem can be mapped to the sedimentation of active particles, which has been studied extensively [46–48]. We exploit that for constant force, the density decays exponentially to very good approximation with sedimentation length
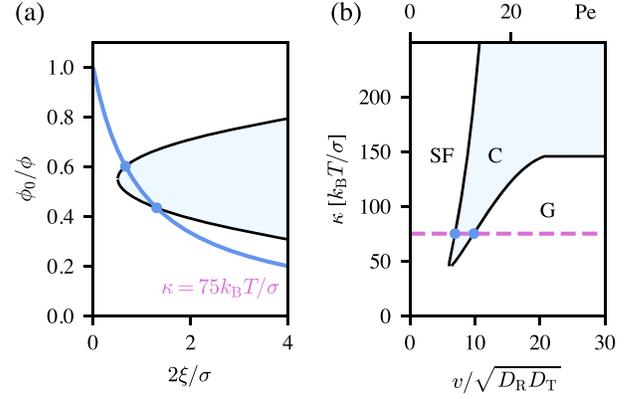

FIG. 5. Prediction from mean-field theory for a straight confined channel of width $g = \sigma$. (a) Filling fraction ϕ_0 (blue line) as a function of sedimentation length ξ. Also shown is the binodal (black line) bounding the coexistence region (shaded area) within which dense clusters coexist with a dilute gas. The force strength is $\kappa = 75 k_B T/\sigma$. The blue dots indicate the range of filling fractions of the force-free region for which the channel exhibits coexistence, which we map to (b) the theoretical phase diagram in the same representation as Fig. 4. The solid line delineates the inhomogeneous cluster regime (C) from single-file behavior (SF) at small speeds and large forces and the weakly confined homogeneous gas (G). The top axis shows the Péclet number estimated using the experimentally measured diffusion coefficients (see the Supplemental Material [31]). Parameters are $v_c = 6\sqrt{D_R D_T}$, $\phi_c = 0.55\phi$, and $\chi = 0.015\sqrt{D_R D_T}\phi$.

$$\xi = \frac{k_B T}{\kappa}\left(1 + \frac{v^2}{2 D_R D_T}\right). \tag{4}$$

This length is reduced as the confining force is increased, whereas APs with larger speed are able to move against the force and to explore a larger area implying larger ξ. We model the density distribution as equal to ρ_0 within a stripe of width g (the force-free region) and to decay as $\rho(y) = \rho_0 e^{-(|y|-g/2)/\xi}$ outside. Normalizing the density leads to a dimensionless filling fraction $\phi_0 = \rho_0\sigma^2 = \phi(g/\sigma + 2\xi/\sigma)^{-1}$ within the force-free gap.

Even though in strict 1D only finite clusters form and complete phase separation is preempted [49,50], we posit that the dynamical instability underlying motility-induced phase separation persists. To expose the basic mechanism without striving for quantitative agreement, we employ the mean-field form [51] of the coexisting filling fractions $\phi_{\pm} = \phi_c \pm \chi\sqrt{v^2 - v_c^2}$ with critical fraction ϕ_c, critical speed v_c, and shape coefficient χ. Figure 5(a) shows the binodal $\phi_{\pm}$ bounding the coexistence region together with ϕ_0 as a function of the sedimentation length ξ. In this representation, ϕ_0 is invariant, but the binodal $\phi_{\pm}$ moves to the left as the confining force κ is increased ($\xi_c \sim 1/\kappa$). Clusters start forming when ϕ_0 crosses ϕ_+ and enters the MIPS coexistence region. Increasing the speed further, APs overcome the confining force and thus effectively reduce

ϕ_0 below ϕ_-, returning the system to the active gas phase [cf. Fig. 2(c)]. The resulting phase diagram in Fig. 5(b) reproduces the salient features of the experiments and simulations, cf. Fig. 4. In particular, there is a range of confining forces κ for which it predicts reentrant behavior as the speed v is increased in agreement with the experiments. This demonstrates that such reentrance is a unique property of soft confinements but not found for hard confinements where the accessible area is independent of activity [19,52,53]. While mean-field theory predicts a sharp binodal, the experiments and simulations in Fig. 4 show a more gradual separation due to finite-size effects in the rather small systems. However, we emphasize that experimental measurements are performed above the critical speed and that such finite-size effects do not change the proposed mechanism.

In summary, we have experimentally studied the clustering of self-propelled colloids in a soft annular-shaped confinement. In agreement with numerical simulations of a minimal model we find that cluster formation is only present in a narrow regime of the confinement strength and the Péclet number; otherwise particles are randomly distributed. This behavior results from a strong coupling of the Péclet number to the radial AP motion which leads to a Pe-dependent change of the effective dimension of the confinement. At low Pe where the APs move in single-file manner, the 1D confinement prevents clustering. At large Pe the increasing radial AP motion reduces the effective particle density which also suppresses clustering (similar to MIPS in two-dimensional systems). Because APs hold great promise as a platform for nanorobotic systems, we hope that our study contributes to the view of how such systems can be operated within soft confinements to promote or suppress clogging [17,23].

---

[1] F. Varnik and T. Franosch, Non-monotonic effect of confinement on the glass transition, J. Phys. Condens. Matter 28, 133001 (2016).

[2] K. Nygård, Colloidal diffusion in confined geometries, Phys. Chem. Chem. Phys. 19, 23632 (2017).

[3] A. B. Grommet, M. Feller, and R. Klajn, Chemical reactivity under nanoconfinement, Nat. Nanotechnol. 15, 256 (2020).

[4] C. Bechinger, R. D. Leonardo, H. Löwen, C. Reichhardt, G. Volpe, and G. Volpe, Active particles in complex and crowded environments, Rev. Mod. Phys. 88, 045006 (2016).

[5] S. Ramaswamy, The mechanics and statistics of active matter, Annu. Rev. Condens. Matter Phys. 1, 323 (2010).

[6] M. E. Cates and J. Tailleur, Motility-induced phase separation, Annu. Rev. Condens. Matter Phys. 6, 219 (2015).

[7] Y. Fily and M. C. Marchetti, Athermal phase separation of self-propelled particles with no alignment, Phys. Rev. Lett. 108, 235702 (2012).

[8] I. Buttinoni, J. Bialke, F. Kummel, H. Löwen, C. Bechinger, and T. Speck, Dynamical clustering and phase separation in suspensions of self-propelled colloidal particles, Phys. Rev. Lett. 110, 238301 (2013).

[9] J. Palacci, S. Sacanna, S. Steinberg, D. J. Pine, and P. M. Chaikin, Living crystals of light-activated colloidal surfers, Science 339, 936 (2013).

[10] G. Liu, A. Patch, F. Bahar, D. Yllanes, R. D. Welch, M. Cristina Marchetti, S. Thutupalli, and J. W. Shaevitz, Self-driven phase transitions drive *Myxococcus xanthus* fruiting body formation, Phys. Rev. Lett. 122, 248102 (2019).

[11] C. Anderson and A. Fernandez-Nieves, Social interactions lead to motility-induced phase separation in fire ants, Nat. Commun. 13, 6710 (2022).

[12] A. Wysocki, R. G. Winkler, and G. Gompper, Cooperative motion of active Brownian spheres in three-dimensional dense suspensions, Europhys. Lett. 105, 48004 (2014).

[13] J. Stenhammar, D. Marenduzzo, R. J. Allen, and M. E. Cates, Phase behaviour of active Brownian particles: The role of dimensionality, Soft Matter 10, 1489 (2014).

[14] F. Turci and N. B. Wilding, Phase separation and multibody effects in three-dimensional active Brownian particles, Phys. Rev. Lett. 126, 038002 (2021).

[15] V. Soni, E. S. Bililign, S. Magkiriadou, S. Sacanna, D. Bartolo, M. J. Shelley, and W. T. M. Irvine, The odd free surface flows of a colloidal chiral fluid, Nat. Phys. 15, 1188 (2019).

[16] F. Moore, J. Russo, T. B. Liverpool, and C. Patrick Royall, Active Brownian particles in random and porous environments, J. Chem. Phys. 158, 104907 (2023).

[17] J. Law, X. Wang, M. Luo *et al.*, Microrobotic swarms for selective embolization, Sci. Adv. 8, eabm5752 (2022).

[18] J. Elgeti and G. Gompper, Wall accumulation of self-propelled spheres, Europhys. Lett. 101, 48003 (2013).

[19] W. Yan and J. F. Brady, The force on a boundary in active matter, J. Fluid Mech. 785, R1 (2015).

[20] H. E. Ribeiro and F. Q. Potiguar, Lane formation and crystallization of active matter in a narrow channel, Physica (Amsterdam) 503A, 849 (2018).

[21] H. Moyses, J. Palacci, S. Sacanna, and D. G. Grier, Trochoidal trajectories of self-propelled Janus particles in a diverging laser beam, Soft Matter 12, 6357 (2016).

[22] T. Vater, M. Isele, U. Siems, and P. Nielaba, Lane and band formation of oppositely driven colloidal particles in two-dimensional ring geometries, Phys. Rev. E 106, 024606 (2022).

[23] L. Abdelmohsen, F. Peng, Y. Tu, and D. A. Wilson, Micro- and nano-motors for biomedical applications, J. Mater. Chem. B 2, 2395 (2014).

[24] P. Dolai, A. Das, A. Kundu, C. Dasgupta, A. Dhar, and K. Vijay Kumar, Universal scaling in active single-file dynamics, Soft Matter 16, 7077 (2020).

[25] I. Mukherjee, A. Raghu, and P. K. Mohanty, Nonexistence of motility induced phase separation transition in one dimension, SciPost Phys. 14, 165 (2023).

[26] G. Gonnella, D. Marenduzzo, A. Suma, and A. Tiribocchi, Motility-induced phase separation and coarsening in active matter, C.R. Phys. 16, 316 (2015).

[27] A. K. Omar, K. Klymko, T. GrandPre, and P. L. Geissler, Phase diagram of active Brownian spheres: Crystallization and the metastability of motility-induced phase separation, Phys. Rev. Lett. 126, 188002 (2021).

[28] A. K. Omar, H. Row, S. A. Mallory, and J. F. Brady, Mechanical theory of nonequilibrium coexistence and

motility-induced phase separation, Proc. Natl. Acad. Sci. U.S.A. **120,** e2219900120 (2023).

[29] C. Lozano, B. T. Hagen, H. Lowen, and C. Bechinger, Phototaxis of synthetic microswimmers in optical landscapes, Nat. Commun. **7,** 12828 (2016).

[30] S. Samin and R. van Roij, Self-propulsion mechanism of active Janus particles in near-critical binary mixtures, Phys. Rev. Lett. **115,** 188305 (2015).

[31] See Supplemental Material at http://link.aps.org/supplemental/10.1103/PhysRevLett.133.048301 for additional information about the experimental methods, a characterization of the experimental setup and additional measurements, which includes Ref. [32].

[32] M. R. Bailey, A. R. Sprenger, F. Grillo, H. Löwen, and L. Isa, Fitting an active Brownian particle's mean-squared displacement with improved parameter estimation, Phys. Rev. E **106,** L052602 (2022).

[33] J. R. Gomez-Solano, S. Samin, C. Lozano, P. Ruedas-Batuecas, R. van Roij, and C. Bechinger, Tuning the motility and directionality of self-propelled colloids, Sci. Rep. **7,** 14891 (2017).

[34] T. Knippenberg, A. Luders, C. Lozano, P. Nielaba, and C. Bechinger, Role of cohesion in the flow of active particles through bottlenecks, Sci. Rep. **12,** 11525 (2022).

[35] Z. Chen, H. Ding, P. S. Kollipara *et al.*, Synchronous and fully steerable active particle systems for enhanced mimicking of collective motion in nature, Adv. Mater. **36,** e2304759 (2023).

[36] G. Volpe, I. Buttinoni, D. Vogt, H.-J. Kümmerer, and C. Bechinger, Microswimmers in patterned environments, Soft Matter **7,** 8810 (2011).

[37] G. Li and J. X. Tang, Accumulation of microswimmers near a surface mediated by collision and rotational Brownian motion, Phys. Rev. Lett. **103,** 078101 (2009).

[38] Y. Fily, A. Baskaran, and M. F. Hagan, Dynamics and density distribution of strongly confined noninteracting nonaligning self-propelled particles in a nonconvex boundary, Phys. Rev. E **91,** 012125 (2015).

[39] N. Nikola, A. P. Solon, Y. Kafri, M. Kardar, J. Tailleur, and R. Voituriez, Active particles with soft and curved walls: Equation of state, ratchets, and instabilities, Phys. Rev. Lett. **117,** 098001 (2016).

[40] J. D. Weeks, D. Chandler, and H. C. Andersen, Role of repulsive forces in determining the equilibrium structure of simple liquids, J. Chem. Phys. **54,** 5237 (1971).

[41] A. Thery, C. C. Maass, and E. Lauga, Hydrodynamic interactions between squirmers near walls: Far-field dynamics and near-field cluster stability, R. Soc. Open Sci. **10,** 230223 (2023).

[42] N. Yoshinaga and T. B. Liverpool, Hydrodynamic interactions in dense active suspensions: From polar order to dynamical clusters, Phys. Rev. E **96,** 020603(R) (2017).

[43] A. Bricard, J. B. Caussin, N. Desreumaux, O. Dauchot, and D. Bartolo, Emergence of macroscopic directed motion in populations of motile colloids, Nature (London) **503,** 95 (2013).

[44] M. Tanemura, Statistical distributions of poisson Voronoi cells in two and three dimensions, Forma **18,** 221 (2003).

[45] E. L. Hinrichsen, J. Feder, and T. Jøssang, Random packing of disks in two dimensions, Phys. Rev. A **41,** 4199 (1990).

[46] F. Ginot, I. Theurkauff, D. Levis, C. Ybert, L. Bocquet, L. Berthier, and C. Cottin-Bizonne, Nonequilibrium equation of state in suspensions of active colloids, Phys. Rev. X **5,** 011004 (2015).

[47] F. Ginot, A. Solon, Y. Kafri, C. Ybert, J. Tailleur, and C. Cottin-Bizonne, Sedimentation of self-propelled Janus colloids: Polarization and pressure, New J. Phys. **20,** 115001 (2018).

[48] S. Hermann and M. Schmidt, Active ideal sedimentation: Exact two-dimensional steady states, Soft Matter **14,** 1614 (2018).

[49] J. Tailleur and M. E. Cates, Statistical mechanics of interacting run-and-tumble bacteria, Phys. Rev. Lett. **100,** 218103 (2008).

[50] R. Soto and R. Golestanian, Run-and-tumble dynamics in a crowded environment: Persistent exclusion process for swimmers, Phys. Rev. E **89,** 012706 (2014).

[51] T. Speck, A. M. Menzel, J. Bialke, and H. Löwen, Dynamical mean-field theory and weakly non-linear analysis for the phase separation of active Brownian particles, J. Chem. Phys. **142,** 224109 (2015).

[52] A. Duzgun and J. V. Selinger, Active Brownian particles near straight or curved walls: Pressure and boundary layers, Phys. Rev. E **97,** 032606 (2018).

[53] T. Speck and R. L. Jack, Ideal bulk pressure of active Brownian particles, Phys. Rev. E **93,** 062605 (2016).